



XFEM-based Fatigue Crack Propagation Analysis on Key Welded Connections of Orthotropic Steel Bridge Deck

Xu Jiang¹ · Kai Sun¹ · Xuhong Qiang² · Dan Li³ · Qiwei Zhang¹

Received: 28 August 2021 / Accepted: 24 November 2022 / Published online: 15 December 2022
© Korean Society of Steel Construction 2022

Abstract

Orthotropic steel decks(OSD's) are prone to fatigue cracking under cyclic loads, especially for rib-to-deck welded connection and rib-to-crossbeam welded connection. To reveal fracturing behaviors of these fatigue-prone sites, a multi-scale model of OSD's specimen is established, including segmental shell-element part and local solid-element configuration. Based on the extended finite element method(XFEM), propagation analysis was carried out in this research. The analysis of stress intensity factor (SIF) shows that the crack at the weld root or weld toe of the rib-to-deck welded connection is a mixed-crack with modes I, II and III, where mode I plays a leading role. Besides, the maximum SIF K_I of the crack at the weld toe is slightly larger than that at the weld root. For rib-to-crossbeam welded connection, the maximum SIF K_I at the weld toe of the U-rib is greater than that at the weld toe of the crossbeam. The analysis of crack propagation shows that the crack growth rate at the weld toe is faster than that at the weld root with the same initial crack size and loading conditions. Similarly, for rib-to-crossbeam welded connection, the crack propagation at the weld toe of U-rib performs faster than that at the weld toe of crossbeam.

Keywords Crack propagation · XFEM · Fatigue-prone sites · OSD's · SIF

1 Introduction

OSD's are widely used in long-span bridges because of the advantages of lightweight and high load-bearing capacity. However, as shown in Fig. 1, the connections of the OSD's are prone to fatigue cracking under traffic cyclic loads, especially for the rib-to-deck welded connection, the rib-to-crossbeam welded connection and the butt welded connection of longitudinal ribs(De Jong, 2004; Dung et al., 2015; Fisher & Barsom, 2016; Kainuma et al., 2016; Liu et al., 2015., Qiang et al., 2023). The cracks of rib-to-deck welded connection and rib-to-crossbeam welded connection could seriously decrease service quality of the structure and it's necessary to reveal the crack propagation

mechanism for further optimization design or maintenance. For rib-to-deck welded connection, there are usually two types of crack propagation paths observed most frequently as shown in Fig. 1(Cheng et al., 2017; Shao et al., 2013; Sim et al., 2009). For rib-to-crossbeam welded connection, weld toe and arc incision in crossbeam are prone to fatigue cracking(Kainuma et al., 2018; Konda et al., 2013; Yokozeki & Miki, 2016; Zhang et al., 2015). To investigate the fatigue fracture of crack, there are usually two numerical simulation methods(Wang et al., 2017; Zhang et al., 2017). One method is based on stress-life curve evaluation method, while the other is based on fracture mechanics method. Based on the state of stress, the fatigue performance can be obtained by S–N curve. However, the S–N curve method neglects initial material defects and fail to describe fatigue crack propagation properly, which is unfavorable in further research.

In recent years, fracture mechanics methods are increasingly used in crack propagation analysis of OSD's (Gupta, 2019; Nagy et al., 2013, 2015; Przywara, 2013). Finite element method is the most powerful tool to solve fracture mechanics problems, but the low efficiency of FEM would be especially obvious when simulating crack propagation (Flemisch et al., 2016; Kanth et al., 2019; Rege & Lemu,

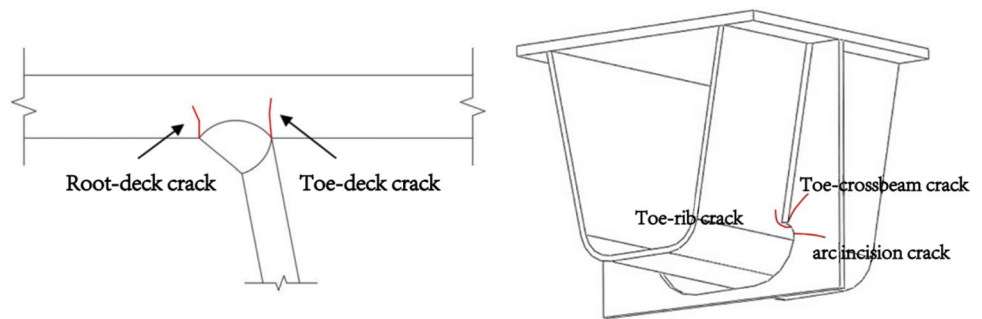
✉ Xuhong Qiang
qiangxuhong@tongji.edu.cn

¹ Department of Bridge Engineering, College of Civil Engineering, Tongji University, Shanghai 200092, China

² Department of Building Engineering, College of Civil Engineering, Tongji University, Shanghai 200092, China

³ Guangzhou Development Zone, Financial Investment Construction Project Management Center, Guangzhou, China

Fig.1 Typical fatigue cracks and their propagation types in OSDs



2017). Based on partition of unity method(PUM)(Melenk & Babuška, 1996), the extended finite element method(XFEM) was first proposed by Belyschko and Black in 1999 (Belytschko & Black, 1999). The discontinuities inside the structure are independent from the grids used, so it is unnecessary to remesh when simulating the evolution of discontinuities. During the following decades, a large number of researches continue to optimize XFEM and verify its effectiveness (Bouhala et al., 2015; Dimitri et al., 2017; Duflo & Bordas, 2008; Laborde et al., 2005; Roth et al., 2015; Xu et al., 2019). After the recorded success in simulating crack propagation, XFEM began to be used in crack propagation analysis of OSD's. Combined XFEM with a full-scale fatigue test, Zhang et al. (Zhang et al., 2018) investigated the crack propagation and fatigue life of the welding details at the longitudinal rib and deck of an orthotropic steel bridge. By taking the uncertainties induced by vehicle loads as well as the defects into account, Wang et al. (Wang et al., 2016) calculated the macro-crack initiation life (MCIL) of OSD's, proving that XFEM is applicable and effective to obtain the variation of the MCIL. More recently, Van et al. (Van et al., 2021) discussed the effects of residual stress on fatigue crack propagation of OSD's based on XFEM. Considering crack tip elastoplastic, Wang et al.(Wang et al., 2021) performed fatigue crack propagation analysis of OSD's.

This paper aims to reveal fracturing behaviors concerning fatigue-prone sites of OSD's, including rib-to-deck welded connection and rib-to-crossbeam welded connection. Based on Sutong Bridge in China, a multi-scale segmental model of OSD's specimen is established, and the SIF is analyzed through XFEM. Besides, crack propagation analysis is carried out for the most unfavorable position, providing guidance for further maintenance of the bridge.

2 FE-Model

The fatigue failure of orthotropic steel bridge deck is mostly located in structural details, where both large-scale model and structural detailed model of the whole bridge could not meet the requirements of model refinement and reasonable

boundary conditions at the same time. Thus, a multi-scale segmental model is established in ABAQUS, consisting of shell-element model of segmental steel box girder and solid-element model of weld detail.

According to the inspection report of Sutong Bridge, there are more cracks in segment NJ22 so it is referenced in the segment model, whose element type is S4R and material Q345qD is selected. Thus Young's modulus is defined as 210000 MPa and Poisson's ratio is 0.3. The standard length of the section is 16 m and 4 standard girder section distances are selected in the longitudinal direction. The steel box girder is 4 m high and 41 m wide (including wind spout), with 14 mm thick deck, 8 mm thick U-rib and 10 mm thick crossbeam, and the longitudinal trusses are set according to the real bridge dimensions.

The rib-to-deck welded connection and rib-to-crossbeam welded connection of No. 17 U-rib are selected as the area of concern, where are under below the heavy wheel track and suffer the most serious fatigue damage. For rib-to-deck welded connection, the size of detailed solid model is 100 mm × 100 mm × 40 mm (length × width × height). As shown in Fig. 2, the thickness of the steel deck is 14 mm, which is the same as that of the real bridge. The size of the weld toe is 8 mm, while the solid element type is C3D8R. When it comes to rib-to-crossbeam welded connection, the size of detailed solid model is 400 mm × 400 mm × 350 mm (length × width × height), where the height of U-rib is 300 mm.

Integrating accuracy and model complexity, the mesh size of the overall shell-element model of the steel box girder is 200 mm, and the size of the encrypted transition at the shell-to-solid boundary is 5 mm. For detailed solid model, the mesh size of rib-to-crossbeam welded connection is 5 mm, and according to the results of mesh sensitivity analysis, the mesh refinement around the cracks is 2 mm, as shown in Figs. 3 and 4.

The standard fatigue vehicle model III in JTG D64-2015(CO, 2015) with a single wheel load of 60kN is taken as the fatigue load when analyzing SIF. As shown in Fig. 5. the standard fatigue vehicle model III consists of four standard axles, and the spacing between the longitudinal

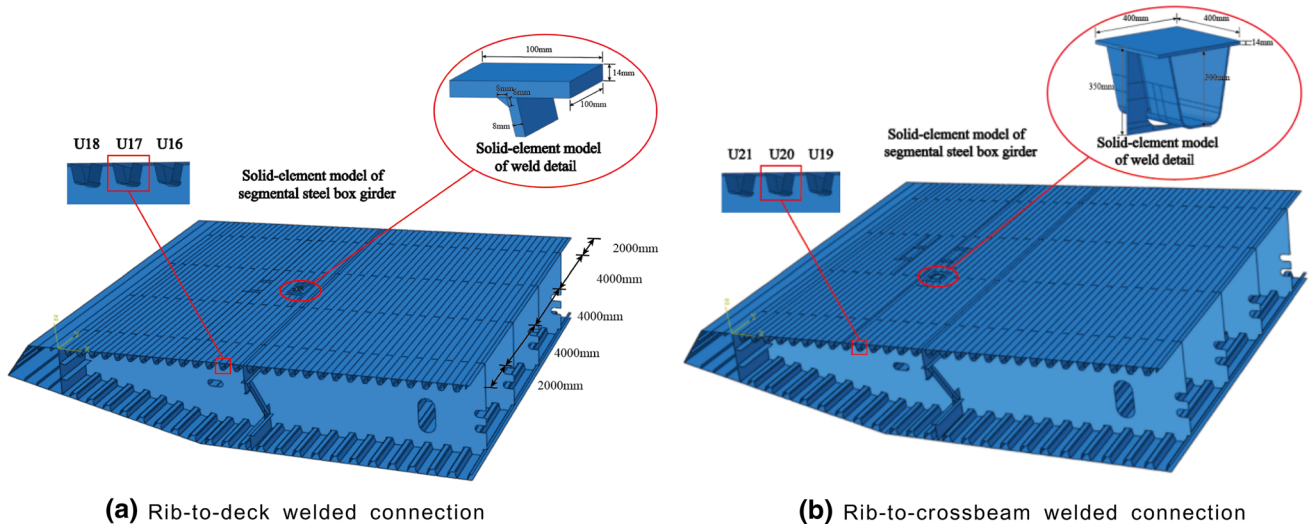


Fig. 2 Finite element models

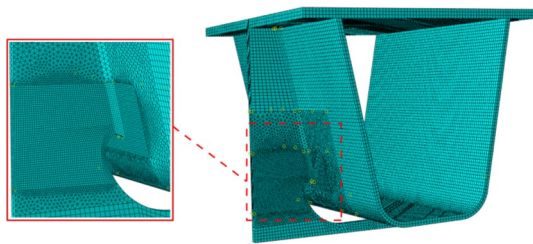


Fig. 3 Mesh generation of detailed solid model

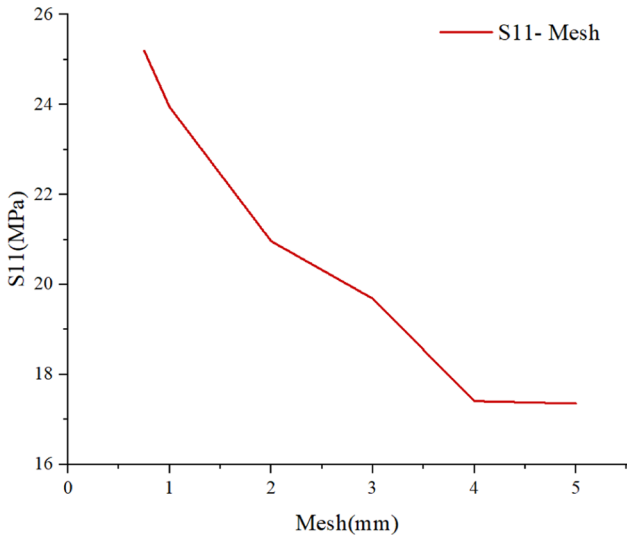


Fig. 4 Mesh sensitivity analysis

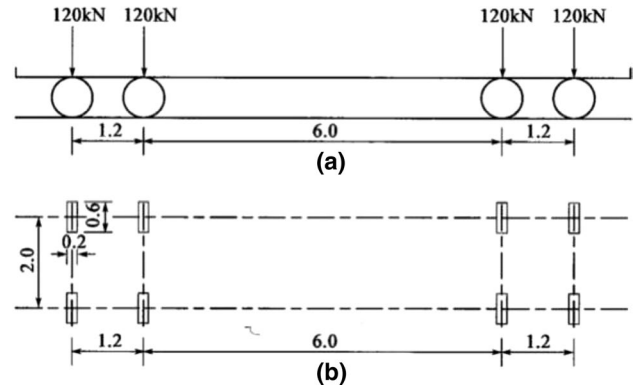


Fig. 5 Fatigue load model III

of 1.2 m is considered as the fatigue load in this paper. Based on the specification, the single wheel landing area is 200 mm × 600 mm.

The fatigue load of ABAQUS model is realized through DLOAD subprogram, with a 200 mm moving step in both the horizontal and vertical directions (with an additional working condition at the vertical center). As shown in Fig. 6, a total of 9 working conditions are set, including HLC1-HLC9 and the gap is 200 mm. Considering the blocking effect of crossbeams, a total of 55 working conditions (ZLC1-ZLC55) are set for rib-to-deck welded connection while 35 (ZLC1-ZLC35) for rib-to-crossbeam welded connection. Distance between adjacent step is 200 mm as well and the detailed layout is illustrated in Fig. 6.

front and rear axle groups is large (6 m). In order to simplify calculation, only the longitudinal axle group spacing

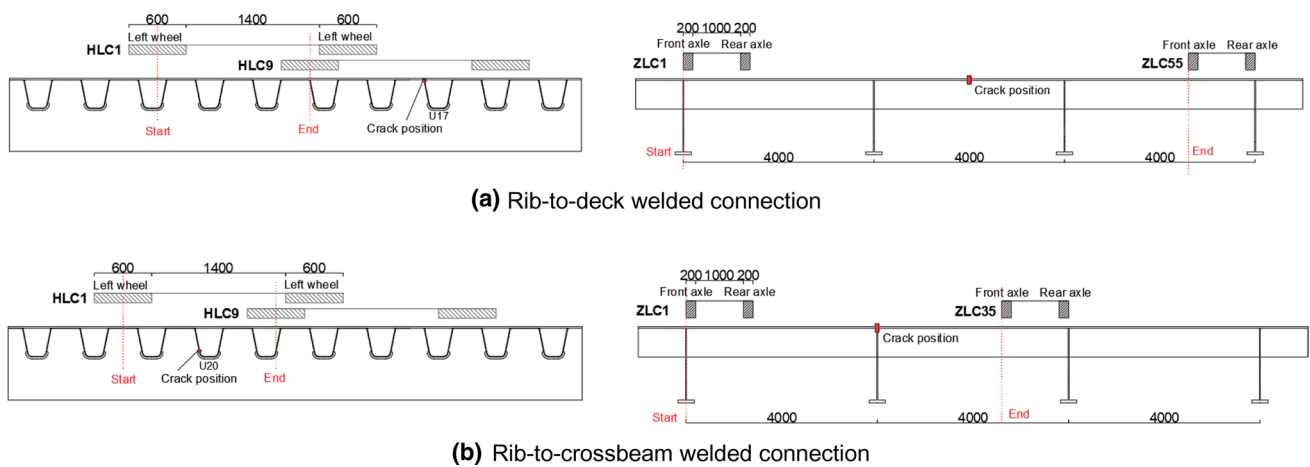


Fig. 6 Detailed loading cases

3 Simulation of crack propagation

Semi-elliptical cracks are introduced to the root and toe of the rib-to-deck welded connection, the weld toe of the rib-to-crossbeam welded connection, weld toe of the U-rib and the arc incision of crossbeam respectively, typical examples are shown in Fig. 7. The crack type is set as XFEM, and the crack expansion option and geometric non-linearity are switched off in the FEM simulation, and "hard contact" is used between the crack and the overall model. The SIF is calculated using the J-integration method, and the first 15

perimeter integrals of the crack tip are output, and the SIF is taken after the integration results are stabilized.

In this work, a three-dimensional crack propagation model of steel box girder is adopted, in which the initial crack is a surface crack. According to the actual crack shape, the surface crack can be assumed as ellipse, semi ellipse or 1/4 ellipse. Considering the initial detectability and semi-ellipse crack (Wang et al., 2019) with a length of 10 mm and a depth of 2.5 mm is used as the initial crack.

Paris formula describing the crack growth rate is expressed as Eq. (1). According to JSSC(Construction(JSSC),

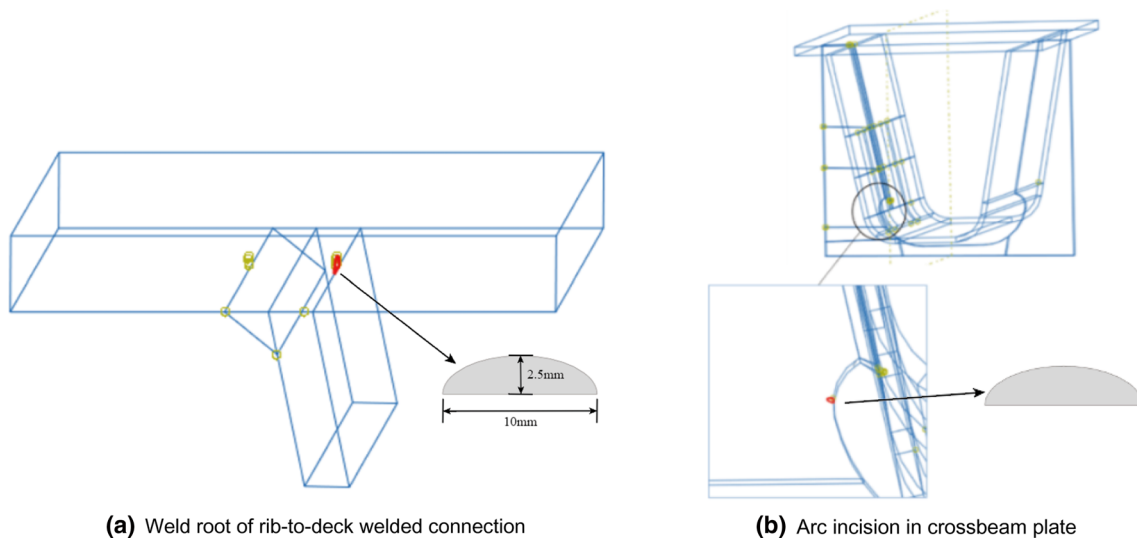


Fig. 7 Semi elliptical cracks

1995) and BS7910 (Standard, 2013), the value of C is 1.5×10^{-11} m/time where m in Eq. (1) is 2.75. The fatigue crack propagation threshold is $\Delta K_{th} = 63 \text{MPa} \cdot \text{mm}^{0.5}$ based on configuration of this type in JTG D64-2015(CO, 2015), and the crack propagation direction is the direction of maximum shear stress.

$$\frac{da}{dN} = c_1(\Delta G)^m \tag{1}$$

4 Analysis of calculation results

4.1 SIF analysis

4.1.1 Rib-to-deck welded connection

Focusing on the longitudinal center position, the SIFs of the rib-to-deck welded connections have been investigated. Among the cracking modes, cracking mode I is the most common and dangerous one and the influence lines of SIF

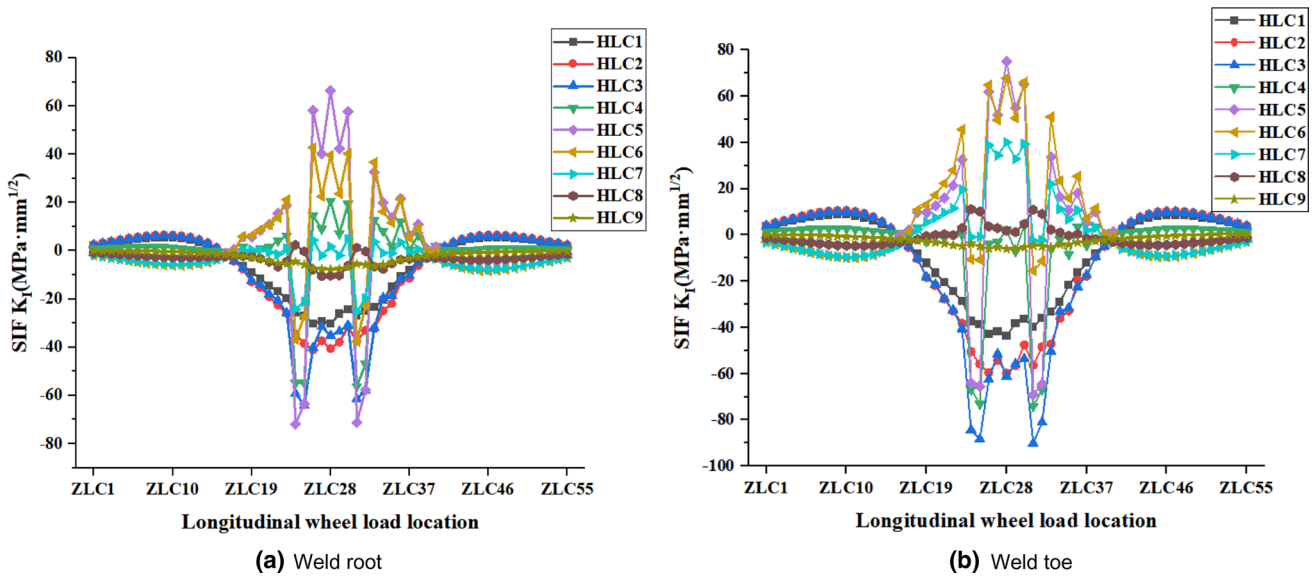


Fig. 8 Influence line of K_I ($\text{MP} \cdot \text{mm}^{1/2}$)

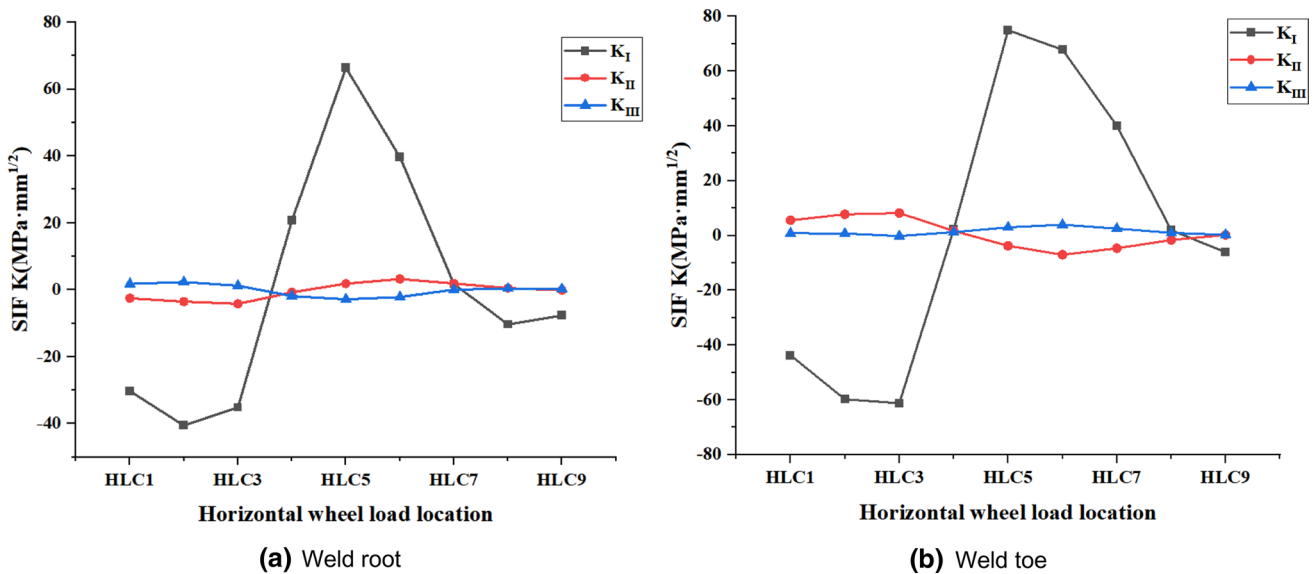


Fig. 9 SIF at longitudinal center ($\text{MP} \cdot \text{mm}^{1/2}$)

K_I under different loading conditions at weld toe and weld root are shown in Fig. 8, which vary between around -80 and 80 MP·mm^{1/2}. In longitudinal direction, when the wheel moves near the observation point, the SIF K_I reaches its peak value, and fluctuates between the maximum values when it is about 1 m away from the center. Compared with weld root, the maximum SIF K_I of the initial crack at weld toe is slightly larger.

The transverse influence lines of SIF K_I , K_{II} and K_{III} at crack tip are illustrated in Fig. 9. When the axle is near the center in longitudinal direction and the wheel is located on the right side of the crack in transverse direction, the cracks at the weld root and weld toe are mainly tensile, which is positive; when the axle is near the center in longitudinal direction and the wheel is located at the left side of the crack in transverse direction, the cracks at the weld root and weld toe are mainly compressed, which is negative.

The longitudinal influence lines of SIF K_I , K_{II} and K_{III} at transverse center position of crack tip are shown in Fig. 10. The SIF K_I of the initial cracks at the rib-to-deck welded connection accounts for the largest proportion among the three kinds of SIFs, and the cracking mode I is dominant in the mixed mode fatigue cracks at the rib-to-crossbeam welding position.

4.1.2 Rib-to-crossbeam welded connection

For connection details of rib-to-crossbeam, the influence lines of SIF K_I under different loading conditions are shown in Fig. 11. For SIF K_I , K_{II} and K_{III} , the transverse and longitudinal influence lines at the crack tip are shown in Figs. 12 and 13 respectively.

The maximum value of SIF K_I at the welding toe of U-rib can reach 200 MPa·mm^{0.5}, which is far more than

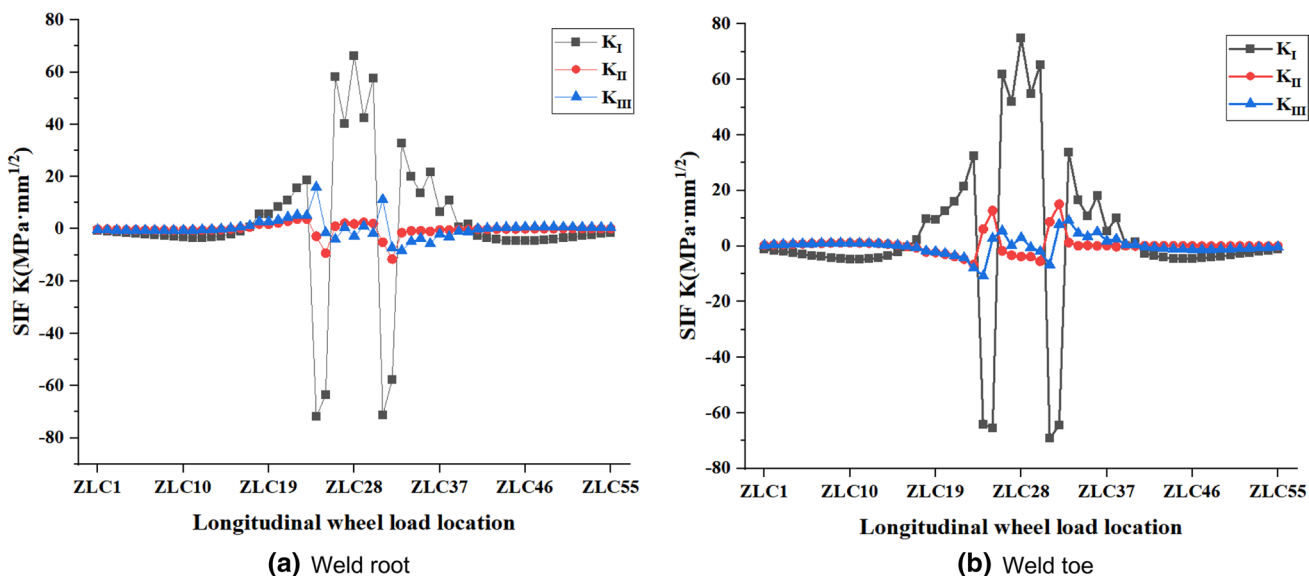


Fig. 10 SIF at transverse center (MP·mm^{1/2})

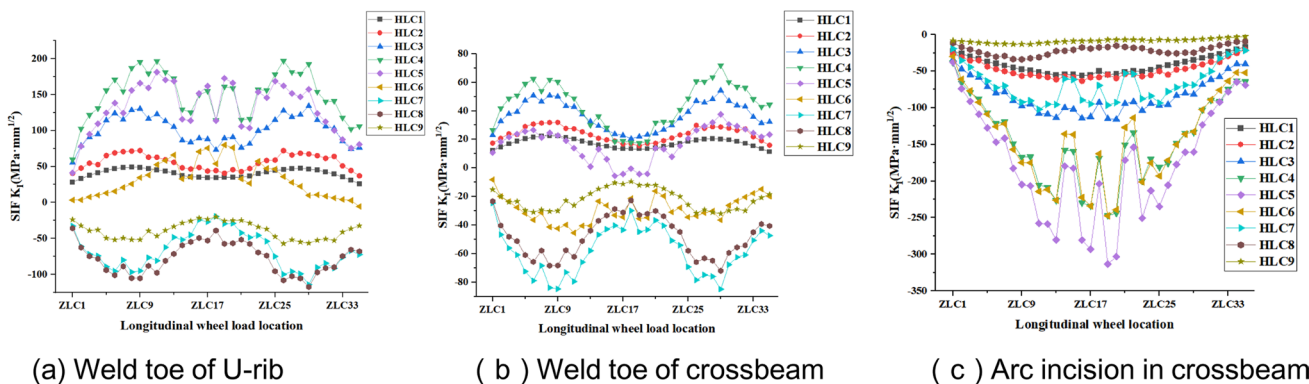


Fig. 11 Influence line of (MP·mm^{1/2})

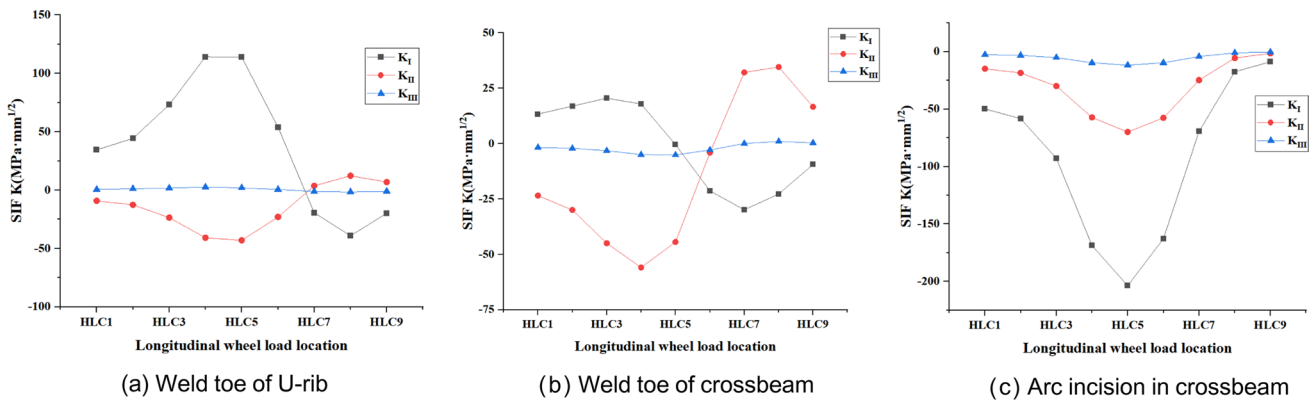


Fig. 12 CSIF at longitudinal center (MPa·mm^{1/2})

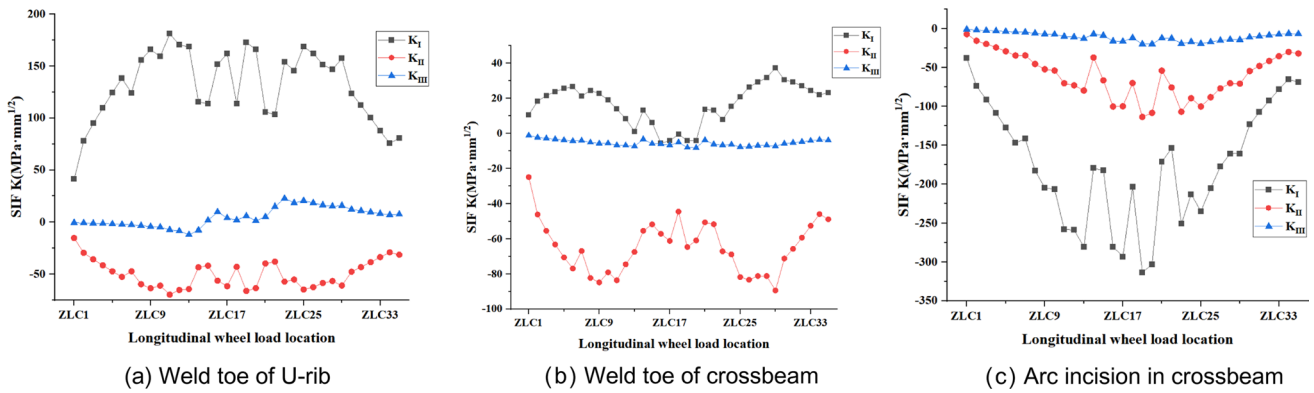


Fig. 13 SIF at transverse center (MPa·mm^{1/2})

the threshold value of the SIF of the steel structure. There is a large driving force for crack propagation, which is greater than the maximum value at the weld toe of the crossbeam. It is consistent with the phenomenon that there are more short cracks at the welding toe of U-rib. Mode I crack is dominant at the weld toe of U-rib, while the mode I and mode II at the weld toe of crossbeam take up a large proportion; the SIF of crossbeam arc notch is negative and the crack is compressed. The residual tensile stress and out of plane deformation at the edge of the arc incision may be the reasons for fatigue cracking, although the initial crack at the arc incision is mostly closed in compression under vehicle load.

The SIF K_I of the initial crack tip at the weld toe of rib-to-crossbeam welded connection reaches its minimum value when the wheel load is located in the longitudinal center,

and reaches maximum at 1.6 m away from longitudinal center.

4.2 Propagation of fatigue crack

4.2.1 Rib-to-deck welded connection

4.2.1.1 Weld root The variation of crack pattern, expansion rate and cumulative strain energy release rate at the weld root of rib-to-deck welded connection during crack propagation are shown in Figs. 14, 15. With the effect of fatigue cycle, the crack continues to expand and Fig. 14(b) shows the relationship between the number of fatigue expansions and the number of cycles. After 10 million loading cycles, the crack extends to 8 mm in depth and 60 mm in length. According to the analysis of cumulative strain energy

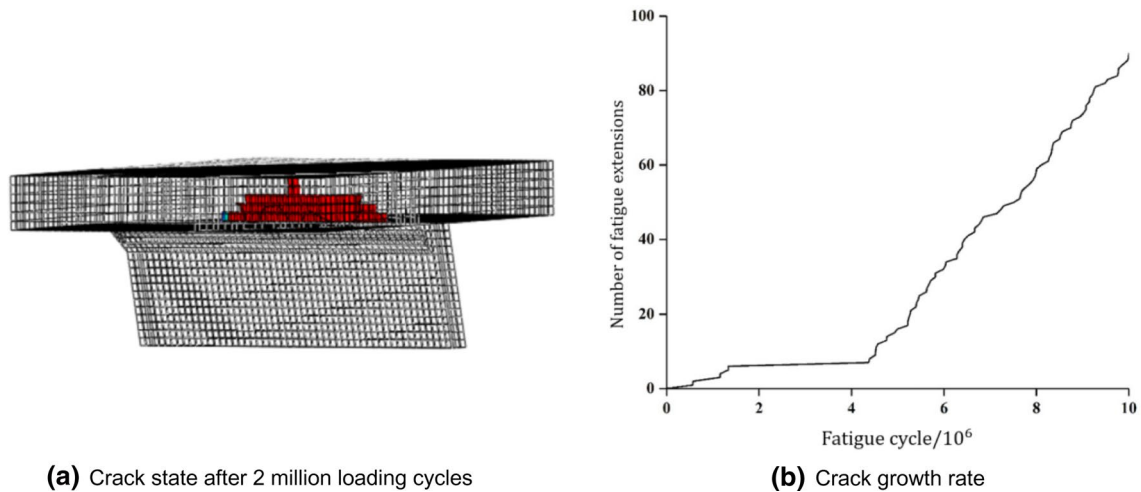


Fig. 14 Crack fatigue propagation

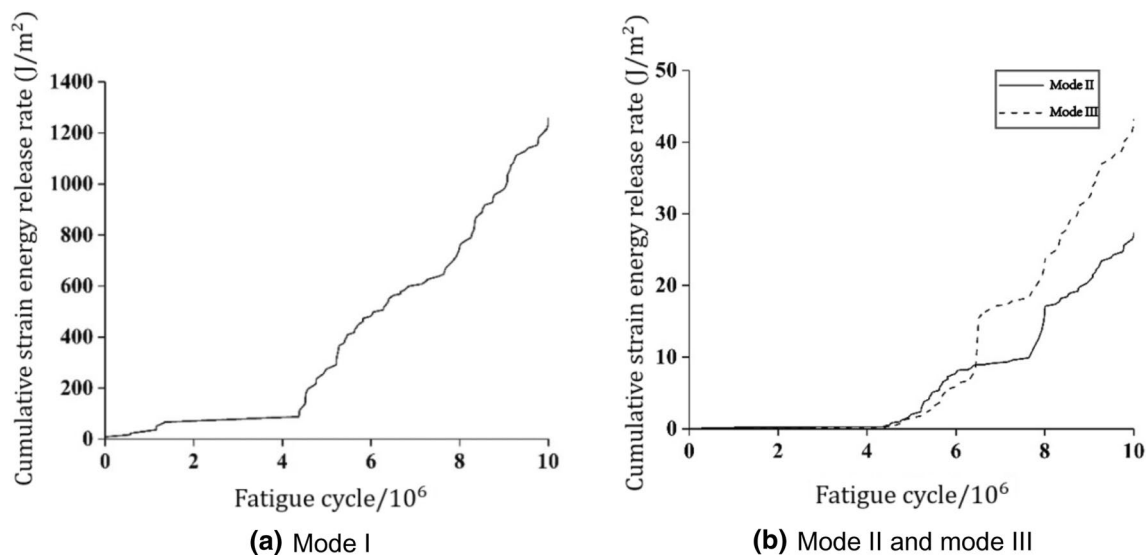


Fig. 15 Cumulative strain energy release rate.

release rate in Fig. 15, it can be seen that during the process mode I is dominant, while mode II and mode III account for only 2.5% respectively and mainly reflected in the direction deflection in the later stage of crack propagation.

The crack at the weld root is almost flat during the propagation process, and its shape is still roughly semi elliptical, while the ratio of long axis to short axis changes constantly. After 4.5 million loading cycles, the crack growth rate increases significantly, and the cumulative strain energy release rate of mode I is about 100J/m². The crack propagates to a depth of 4 mm and a length of 30 mm.

4.2.1.2 Weld toe The variation of crack morphology, growth rate and cumulative strain energy release rate at the

weld toe of rib-to-deck welded connection during crack propagation are shown in Figs. 16, 17. After 2 million loading cycles, the crack surface extends to 8 mm in depth and 70 mm in length. According to the analysis of cumulative strain energy release rate in Fig. 17, it can be seen that G_I is dominant during the process, while G_{II} and G_{III} are nearly equivalent to each other. The growth rate is significantly accelerated after around 1.1 million loading cycles, mainly reflected in the direction deflection in the later stage of crack growth. The existence of mode II and mode III cracks will accelerate the crack growth and affect the direction of crack surface, which is important.

The cracks at the weld toe mainly extend along the longitudinal axis of the semi elliptical initial crack, and deflect

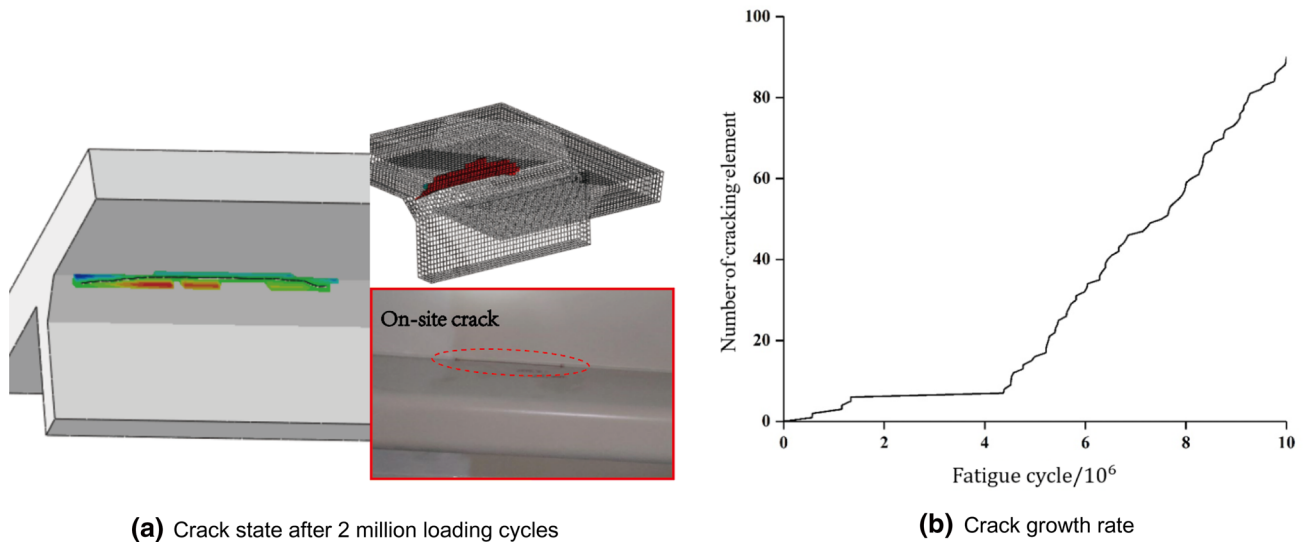


Fig. 16 Crack fatigue propagation

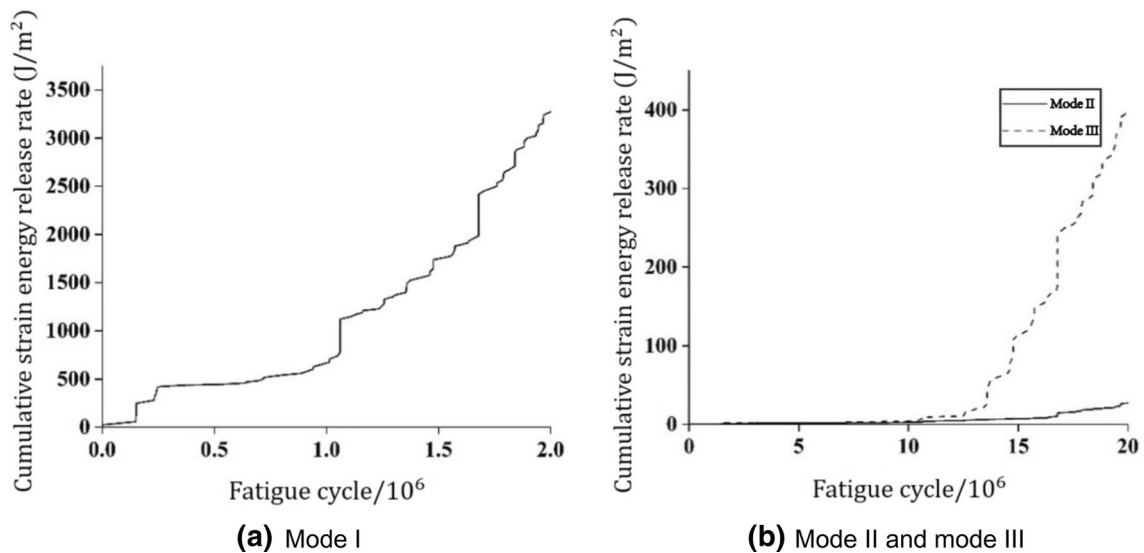


Fig. 17 Cumulative strain energy release rate

towards the weld in the later stage of the propagation. The growth speed is apparently accelerated after 1.1 million cycles, and the cumulative strain energy release rate of type I, which accounts for the largest proportion, is about $800\text{J}/\text{m}^2$, and the crack propagation depth is 8 mm and the length is 34 mm.

4.2.2 Rib-to-crossbeam welded connection

4.2.2.1 Weld toe of U-rib The variation of crack morphology, growth rate and cumulative strain energy release rate at the weld toe of U-rib during crack propagation are shown in Figs. 18, 19. After 200,000 loading cycles, the crack surface

penetrated through the U-rib thickness in depth direction and extended to 54 mm in length direction. The crack at the welding toe of U-rib propagates along the thickness direction of U-rib first, and then propagates along the longitudinal direction. In the later stage of the propagation process, the crack surface deflects slightly vertically upward, and the mode I crack is dominant during the propagation process.

The crack at the welding toe of U-rib propagates rapidly during the early stage, and slows down with the passivation of crack tip when it reaches 4 mm in thickness direction and 20 mm in length. The rapid increase is due to the fact that the crack propagation is in an ascending stage and the difference between the K value and the threshold value

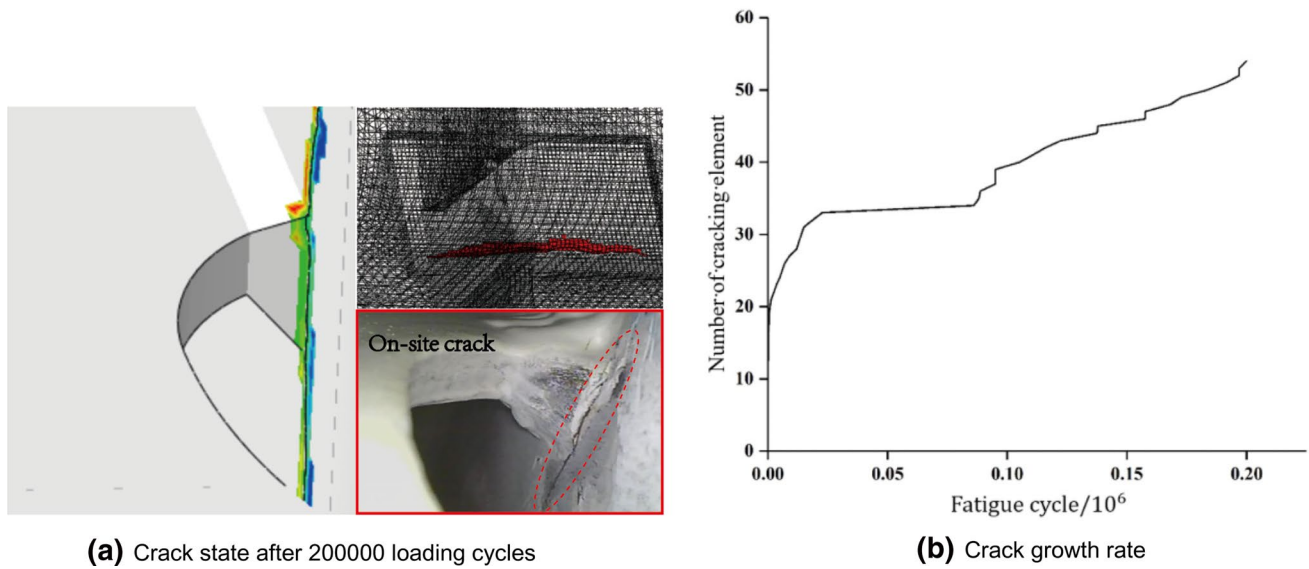


Fig. 18 Crack fatigue propagation

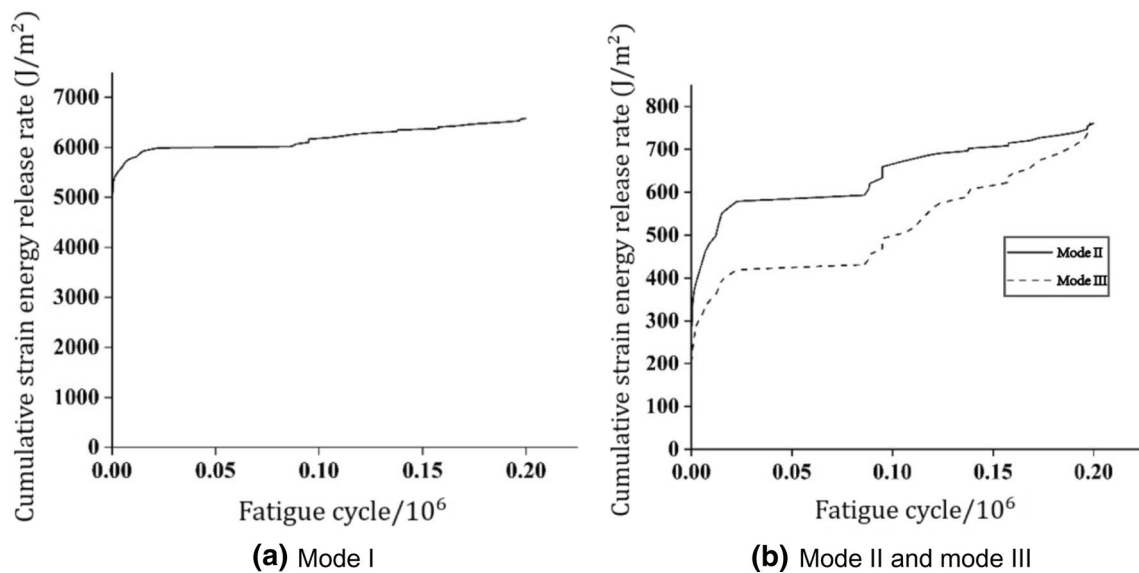
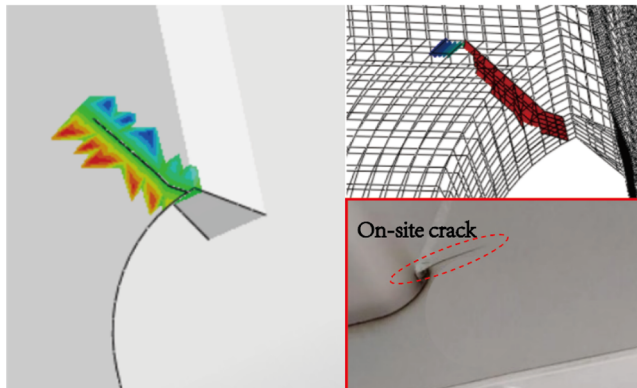


Fig. 19 Cumulative strain energy release rate

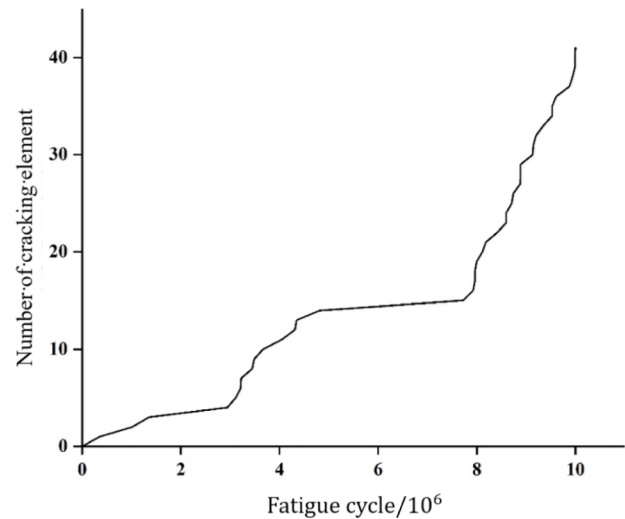
becomes larger as the crack extends. When crack expansion reaches a certain stage, for example expansion into a region of force stability, the K value decreases and crack expansion enters a plateau phase, which could be described as crack tip passivation as well. At this time, the cumulative strain energy release rate of mode I, which accounts for the largest proportion, reaches 5500 J/m^2 , and its speed slows down in the later stage. It is speculated that the discontinuity of geometric structure causes a larger crack growth rate in the

early stage, and decreases gradually after releasing a certain displacement.

4.2.2.2 Weld toe of crossbeam The variation of crack morphology, growth rate and cumulative strain energy release rate at weld toe of crossbeam during crack propagation are shown in Figs. 20, 21. After 10 million loading cycles, the length of crack surface extends to 25 mm along the crossbeam, and penetrates through the crossbeam. There is a cer-



(a) Crack state after 2 million loading cycles



(b) Crack growth rate

Fig. 20 20 Crack fatigue propagation

tain angle between the initial crack and the weld. During the process of crack propagation, the crack propagates along the crossbeam laterally first, and then propagates along the thickness direction of the crossbeam. The propagation direction is basically the same as that of the initial crack. The cumulative strain energy release rate during crack propagation is shown in Fig. 21. It can be seen that the strain energy release rate G_I is relatively small, while G_I and G_{II} develops rapidly in the later stage and becomes dominant. The crack form is related to the stress conditions of this part and out of plane deformation.

The crack growth rate increases significantly after about 8 million loading cycles, and the mode II cumulative strain

energy release rate, which accounts for the largest proportion, reaches 130 J/m^2 . The crack propagates to 6 mm in thickness direction and 20 mm along the crossbeam. By revealing the characteristics of crack propagation at the key positions, it provides a theoretical basis for the monitoring and maintenance of orthotropic steel deck. Through comparison, the development stage of the actual crack could be obtained, and the crack is classified and then the corresponding measures could be taken. As shown in Figs. 20, 21, when reaching 4 million fatigue cycles, initial crack at the weld root of rib-to-deck welded connection will encounter a rapid growth soon, which means a proper repair is necessary.

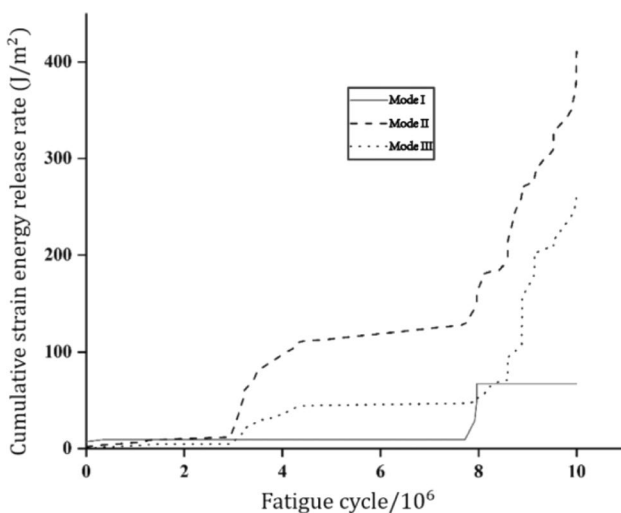


Fig. 21 Cumulative strain energy release rate

5 Conclusions

In this paper, a multi-scale segment model is subjected to dynamic load under the most unfavorable loading condition to simulate the crack growth process. The initial crack is introduced into refined model of typical fatigue parts, and the SIF influence lines of the initial crack tip under vehicle load are calculated. Under the most unfavorable loading condition, the steel box girder segment model was loaded cyclically to simulate the crack propagation process. The following conclusions can be drawn:

For both rib-to-deck welded connection and rib-to-crossbeam welded connection, mode I fatigue crack growth plays a leading role in the mixed-mode crack of 3 modes at the weld root and weld toe. In contrast, the maximum SIF K_I of the crack at the weld toe is slightly greater than that of the crack at the weld root.

For the fatigue detail of rib-to-deck welded connection, the crack propagates longitudinally along the weld direction, and then turns to the depth direction. Besides, the propagation rate increases gradually and the crack keeps plane during the propagation.

For rib-to-crossbeam welded connection, the crack at the weld toe of the U-rib propagates along the crack width and depth directions in the U-rib, while the crack at the weld toe of the crossbeam propagates along the crossbeam thickness direction and the crossbeam surface, both of which are consistent with the actual situation.

When the initial crack size and the loading condition are same, the crack growth rate at the weld toe is faster than that at the weld root. Similarly, the crack propagation rate at the weld toe of U-rib is faster than that at the weld toe of crossbeam.

The results of this research can be used as a source of reference, when rehabilitation strategy of orthotropic steel bridge decks is proposed. Based on comparison of actual crack and FEM results, the development stage of the crack is classified and then the corresponding measures could be taken.

Funding The authors gratefully acknowledge the financial supports provided by the Key Research Project of Guangdong Province of China (2019B111106002), Scientific research project of Shuohuang Railway Development Co., Ltd (SHGF-18-50), the National Natural Science Foundation of China (52278207), the Natural Science Foundation of Shanghai (Grant No. 21ZR1466100).

Declarations

Conflicts of interest There are no conflicts of interest.

References

- Belytschko, T., & Black, T. (1999). Elastic crack growth in finite elements with minimal remeshing. *International Journal for Numerical Methods in Engineering*, 45(5), 601–620.
- Bouhala, L., Makradi, A., & Belouettar, S. (2015). Thermo-anisotropic crack propagation by XFEM. *International Journal of Mechanical Sciences*, 103, 235–246.
- Cheng, B., Ye, X., Cao, X., Mbako, D. D., & Cao, Y. (2017). Experimental study on fatigue failure of rib-to-deck welded connections in orthotropic steel bridge decks. *International Journal of Fatigue*, 103, 157–167.
- Co H C (2015). Specifications for Design of Highway Steel Bridge (JTG D64–2015).
- Construction (Jssc) J S O S (1995). Fatigue design recommendations for steel structures and commentary.
- Dimitri, R., Fantuzzi, N., Li, Y., & Tornabene, F. (2017). Numerical computation of the crack development and SIF in composite materials with XFEM and SFEM. *Composite Structures*, 160, 468–490.
- Duflot, M., & Bordas, S. (2008). A posteriori error estimation for extended finite elements by an extended global recovery. *International Journal for Numerical Methods in Engineering*, 76(8), 1123–1138.
- Dung, C. V., Sasaki, E., Tajima, K., & Suzuki, T. (2015). Investigations on the effect of weld penetration on fatigue strength of rib-to-deck welded joints in orthotropic steel decks. *International Journal of Steel Structures*, 15(2), 299–310.
- Fisher, J. W., & Barsom, J. M. (2016). Evaluation of cracking in the rib-to-deck welds of the Bronx-Whitestone Bridge. *Journal of Bridge Engineering*, 21(3), 04015065.
- Flemisch, B., Fumagalli, A., & Scotti, A. (2016). A review of the XFEM-based approximation of flow in fractured porous media. *Advances in Discretization Methods*, 16, 47–76.
- Gupta R S (2019). Prediction of Fatigue Crack Propagation in Orthotropic Steel Decks using XFEM based on LEFM and VCCT.
- De Jong F (2004). Overview fatigue phenomenon in orthotropic bridge decks in the Netherlands.
- Kainuma, S., Yang, M., Jeong, Y.-S., Inokuchi, S., Kawabata, A., & Uchida, D. (2016). Experiment on fatigue behavior of rib-to-deck weld root in orthotropic steel decks. *Journal of Constructional Steel Research*, 119, 113–122.
- Kainuma, S., Yang, M., Jeong, Y.-S., Inokuchi, S., Kawabata, A., & Uchida, D. (2018). Fatigue Behavior Investigation and Stress Analysis for Rib-to-Deck Welded Joints in Orthotropic Steel Decks. *International Journal of Steel Structures*, 18(2), 512–527.
- Kanth, S. A., Lone, A. S., Harmain, G., & Jameel, A. (2019). Elasto Plastic Crack Growth by XFEM: A Review. *Materials Today: Proceedings*, 18, 3472–3481.
- Konda, N., Nishio, M., Ichimiya, M., Kasugai, T., & Kiyokawa, S. (2013). Development of fatigue test method and improvement of fatigue life by new functional steel plates for welding of trough rib and deck plate of orthotropic decks. *International Journal of Steel Structures*, 13(1), 191–197.
- Laborde, P., Pommier, J., Renard, Y., & Salaün, M. (2005). High-order extended finite element method for cracked domains. *International Journal for Numerical Methods in Engineering*, 64(3), 354–381.
- Liu, R., Ji, B., Wang, M., Chen, C., & Maeno, H. (2015). Numerical evaluation of toe-deck fatigue in orthotropic steel bridge deck. *Journal of Performance of Constructed Facilities*, 29(6), 04014180.
- Melenk, J. M., & Babuška, I. (1996). The partition of unity finite element method: Basic theory and applications. *Computer Methods in Applied Mechanics and Engineering*, 139(1–4), 289–314.
- Nagy W, De Backer H, Van Bogaert P. (2013). Fracture mechanics as an improvement of fatigue life assessment in orthotropic bridge decks. 211–212
- Nagy, W., Van Bogaert, P., & De Backer, H. (2015). LEFM based fatigue design for welded connections in orthotropic steel bridge decks. *Procedia Engineering*, 133, 758–769.
- Przywara, J. (2013). *Applications of the Extended Finite Element Method (XFEM) for the Analysis of Distortion-Induced Fatigue Cracking in Highway Bridge Girders* (pp. 20–51). Lawrence: University of Kansas.
- Qiang, X. H., Shu, Y., & Jiang, X. (2023). Mechanical behaviour of high strength steel T-stubs at elevated temperatures: Experimental study. *Thin-walled Structures*, 182, 110314. <https://doi.org/10.1016/j.tws.2022.11>
- Rege, K., & Lemu, H. (2017). *A review of fatigue crack propagation modelling techniques using FEM and XFEM* (p. 012027). Bristol: IOP Publishing.
- Roth, S.-N., Léger, P., & Soulaïmani, A. (2015). A combined XFEM–damage mechanics approach for concrete crack propagation. *Computer Methods in Applied Mechanics and Engineering*, 283, 923–955.
- Shao, X., Yi, D., Huang, Z., Zhao, H., Chen, B., & Liu, M. (2013). Basic performance of the composite deck system composed of

- orthotropic steel deck and ultrathin RPC layer. *Journal of Bridge Engineering*, 18(5), 417–428.
- Sim, H.-B., Uang, C.-M., & Sikorsky, C. (2009). Effects of fabrication procedures on fatigue resistance of welded joints in steel orthotropic decks. *Journal of Bridge Engineering*, 14(5), 366–373.
- Standard B (2013). BS 7910: 2013. Guide to Methods for Assessing the Acceptability of Flaws in Metallic Structures. Londyn: BSI. pp 20
- Van Den Berg, N., Xin, H., Veljkovic, M. J. M., & Design,. (2021). Effects of residual stresses on fatigue crack propagation of an orthotropic steel bridge deck. *Material Design*, 198, 109294.
- Wang, B., De Backer, H., & Chen, A. (2016). An XFEM based uncertainty study on crack growth in welded joints with defects. *Theoretical and Applied Fracture Mechanics*, 86, 125–142.
- Wang, C., Duan, L., Zhai, M., Zhang, Y., & Wang, S. (2017). Steel bridge long-term performance research technology framework and research progress. *Advances in Structural Engineering*, 20(1), 51–68.
- Wang, Y., Wang, Z., & Zheng, Y. (2019). Analysis of fatigue crack propagation of an orthotropic bridge deck based on the extended finite element method. *Advances in Civil Engineering*, 20, 109–124.
- Wang, Y., Yan, Z., & Wang, Z. (2021). Fatigue Crack Propagation Analysis of Orthotropic Steel Bridge with Crack Tip Elastoplastic Consideration. *Cmes-Computer Modeling in Engineering & Sciences*, 127(2), 549–574.
- Xu, J., Sun, H., Xie, Z., & Sun, J. (2019). Fatigue Behaviour Study of the Shear Stud Using Crack Box Technology and M Integral Method. *International Journal of Steel Structures*, 19(4), 1249–1259.
- Yokozeki, K., & Miki, C. (2016). Fatigue evaluation for longitudinal-to-transverse rib connection of orthotropic steel deck by using structural hot spot stress. *Welding in the World*, 60(1), 83–92.
- Zhang, Q., Bu, Y., & Li, Q. (2017). Review on fatigue problems of orthotropic steel bridge deck. *China Journal of Highway and Transport*, 30(3), 14–30.
- Zhang, Q.-H., Cui, C., Bu, Y.-Z., Liu, Y.-M., & Ye, H.-W. (2015). Fatigue tests and fatigue assessment approaches for rib-to-diaphragm in steel orthotropic decks. *Journal of Constructional Steel Research*, 114, 110–118.
- Zhang, Q., Jin, Z., Liu, Y., & Bu, Y. (2018). 3-D Simulation method for fatigue crack propagation in rib-to-deck welded joints of orthotropic steel bridge deck. *China Journal of Highway and Transport*, 31(1), 57–66.

Publisher's Note Springer Nature remains neutral with regard to jurisdictional claims in published maps and institutional affiliations.

Springer Nature or its licensor (e.g. a society or other partner) holds exclusive rights to this article under a publishing agreement with the author(s) or other rightsholder(s); author self-archiving of the accepted manuscript version of this article is solely governed by the terms of such publishing agreement and applicable law.